Substitution Method for the Analysis of Systems Based on Two Nonlinear Resonators

Almudena Suárez, *Fellow, IEEE*, and Franco Ramírez, *Senior Member, IEEE*

***Abstract*— Circuits containing two nonlinear resonators have recently been proposed for nonreciprocal isolators, robust wireless power transfer, and sensors. A fundamental characteristic is the presence of hysteresis, associated with points of infinite slope in the solution curves. However, the prediction of hysteresis in the presence of the two distinct resonators is not possible in default harmonic balance (HB) and the additional use of continuation techniques may not be exhaustive enough. Here, we present a novel substitution method, based on the use of two auxiliary generators (AGs), that enables the system control through a single excitation voltage. A simple condition is also provided to obtain all the existing loci of infinite-slope points. The methods, which are compatible with commercial HB, will be illustrated through their application to a Lorentzian–Fano nonlinear isolator.**

***Index Terms*— Auxiliary generators (AGs), contour intersections hysteresis, nonlinear resonator.**

I. Introduction

SEVERAL recent works make use of circuits based on two nonlinear resonators for a variety of applications that include nonlinear isolators [1], [2], [3], robust wireless power transfer [4], and sensors [5]. A fundamental characteristic is the presence of hysteresis, associated with multivalued responses. Default harmonic balance (HB) fails to provide the turning points that delimit the hysteresis loops, where the Jacobian matrix of the HB system is singular [6], [7], [8], [9]. There can be a convergence failure or a jump to a distinct curve section. Due to the system ill-conditioning, the jumps may occur relatively far from the turning point, so the prediction of the hysteresis loop will not be reliable. Turning points may be circumvented in in-house software using continuation methods, which basically rely on the replacement of the original parameter with one with respect to which the system is not singular [7], [8]. In commercial software, this can be carried out with the aid of an auxiliary generator (AG) [9], optimized to fulfill a non-perturbation condition, given by the zero value of the ratio between the AG current and voltage. However, when having two nonlinear resonators, the multivalued section(s) will generally be due to the interaction between them. Thus, one AG per nonlinear element is required, which implies fulfilling two non-perturbation conditions in terms of four real state variables, as done, for instance, in [10] and [11]. In the presence of strong nonlinearities, one can expect little accuracy as well as convergence failures.

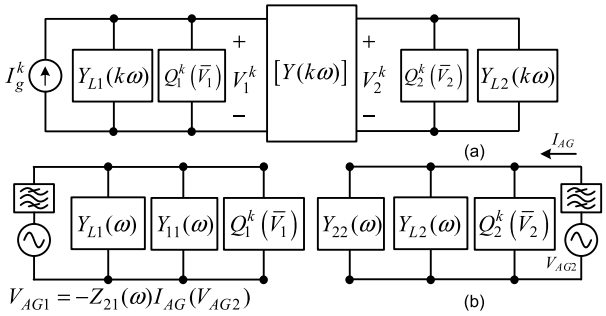

Fig. 1. (a) HB system and (b) setup used for the calculation of the function $H(V_{\mathrm{AG2}})$ defined in (7). This is based on the introduction into the circuit of an independent voltage AG (AG_2) and a current-controlled voltage AG (AG_1). This setup operates at the fundamental frequency only. For the rest of the harmonic terms, the circuit/schematic has no modifications.

A completely different approach was proposed in [12], which is applicable in the presence of a single nonlinear device. It relies on the calculation of a nonlinear admittance/impedance function, obtained by exciting the device with an AG. The system solutions are obtained from contour plots [13] of the defined function. The advantage of the method is that it exhaustively provides all the solutions coexisting for a given set of element values and parameters, which may belong to different curve sections and even to disconnected curves. However, the method can only be applied to circuits containing a single nonlinear device.

This work presents a new analysis method, applicable to circuits containing two distinct nonlinear devices. It is based on the combined use of an independent voltage AG and a current-controlled voltage AG, presented here for the first time. This variable reduction is achieved through a substitution method, applied to the outer-tier system that describes the coupled system at the fundamental frequency. The inner tier is constituted by the pure HB system. The combined use of the two AGs enables the system control with a single independent voltage. The method is compatible with commercial HB.

II. Steady-State System

For the sake of simplicity, we will particularize the formulation to the case of two nonlinear charges, Q_1 and Q_2, connected through a passive-linear admittance matrix $[Y]$ [see Fig. 1(a)]. The system, driven by an input current source I_g at the frequency ω, will be formulated in piecewise HB considering NH harmonic terms

$$\begin{aligned}[Y_{11}(k\omega)+Y_{L1}(k\omega)]V_1^k+Y_{12}(k\omega)V_2^k+jk\omega Q_1^k(\overline{V}_1)=I_g^k\\ Y_{21}(k\omega)V_1^k+[Y_{22}(k\omega)+Y_{L2}(k\omega)]V_2^k+jk\omega Q_2^k(\overline{V}_2)=0\end{aligned} \quad (1)$$

Manuscript received 28 February 2023; accepted 3 April 2023. This work was supported by the Spanish Ministry of Science and Innovation (MCIN/AEI/10.13039/501100011033) under Grant PID2020-116569RB-C31. *(Corresponding author: Franco Ramírez.)*

The authors are with the Departamento de Ingeniería de Comunicaciones, Universidad de Cantabria, 39005 Santander, Spain (e-mail: almudena.suarez@unican.es; ramirezf@unican.es).

This article was presented at the IEEE MTT-S International Microwave Symposium (IMS 2023), San Diego, CA, USA, June 11–16, 2023.

Color versions of one or more figures in this letter are available at https://doi.org/10.1109/LMWT.2023.3264991.

Digital Object Identifier 10.1109/LMWT.2023.3264991

where k goes from $-$NH to NH, $Q_i^k(\overline{V}_i)$ is the kth harmonic component of the nonlinear charge Q_i, with $i = 1, 2$, the vector $\overline{V}_i$ contains the harmonic components of its control voltage, $Y_{k,m}$ are the elements of $[Y]$ and Y_{Li} are other possible passive-linear admittances. To facilitate the description, we will focus on the equations at the fundamental frequency

$$[Y_{11}(\omega)+Y_{L1}(\omega)]V_1^1+Y_{12}(\omega)V_2^1+j\omega Q_1^1(V_1^1,\overline{V}_1')=I_g e^{j\phi} \tag{2a}$$

$$Y_{21}(\omega)V_1^1+[Y_{22}(\omega)+Y_{L2}(\omega)]V_2^1+j\omega Q_2^1(V_2^1,\overline{V}_2')=0 \tag{2b}$$

where $\overline{V}_i'$, with $i = 1, 2$, contains all the harmonic terms of the corresponding control voltage except that at ω. The analysis will be based on a substitution procedure, implemented by means of two AGs. We solve (2b) for V_1^1 in terms of V_2^1 and replace its value in (2a). To this end, we introduce a voltage AG (denoted as AG_2) in parallel with Q_2 [see Fig. 1(b)]. Note that the voltage AG has an ideal bandpass filter in series to prevent it from short-circuiting the harmonic terms. AG_2 operates at ω, with the amplitude V_{AG2}. Due to its connection in parallel with the nonlinear charge, we can make $V_2^1 = V_{AG2}$. Thus, after the introduction of the forcing AG_2, we can write (2b) as

$$Y_{21}(\omega)V_1^1+[Y_{22}(\omega)+Y_{L2}(\omega)]V_{AG2}+j\omega Q_2^1\left(V_{AG2},\overline{V}_2'\right)=0. \tag{3}$$

Note that the pure HB system acts like an inner tier. Assembling terms in (3) we can calculate the following current:

$$I_{AG}=[Y_{22}(\omega)+Y_{L2}(\omega)]V_{AG2}+j\omega Q_2^1\left(V_{AG},\overline{V}_2'\right). \tag{4}$$

And from (3), the voltage V_1^1 must fulfill

$$V_1^1=-I_{AG}/Y_{21}(\omega)=-Z_{21}(\omega)I_{AG}(V_{AG2}) \tag{5}$$

where the dependence on $\overline{V}_2'$ has been dropped just for clarity. To address (2a), we will connect a second voltage AG (AG_1) in parallel with the first nonlinear charge [see Fig. 1(b)]. This AG will provide the following complex voltage at ω:

$$V_{AG1}=-Z_{21}(\omega)I_{AG}(V_{AG2}). \tag{6}$$

Now, at the fundamental frequency ω we have the following complex equation in the two independent variables V_{AG2} and ϕ:

$$\begin{aligned}H(V_{AG2}) &= [Y_{11}(\omega)+Y_{L1}(\omega)][-Z_{21}(\omega)I_{AG}(V_{AG2})]\\ &\quad + Y_{12}(\omega)V_{AG2}+j\omega Q_1^1([-Z_{21}(\omega)I_{AG}(V_{AG2})])\\ &= I_g e^{j\phi}\end{aligned} \tag{7}$$

where the dependence on $\overline{V}_1'$ has also been dropped. By calculating the magnitude of $H(V_{AG2})$, we will have

$$\left|\begin{aligned}&[Y_{11}(\omega)+Y_{L1}(\omega)][-Z_{21}(\omega)I_{AG}(V_{AG2})]+Y_{12}(\omega)V_{AG2}\\ &+j\omega Q_1^1\left([-Z_{21}(\omega)I_{AG}(V_{AG2})],\overline{V}_1'\right)\end{aligned}\right|=I_g. \tag{8}$$

In a practical simulation, we will introduce into the circuit the independent voltage source AG_2 and the current-controlled voltage source AG_1. We will sweep V_{AG2} and perform an HB analysis at each sweep step. Then, we will calculate I_g using the function $H(V_{AG2})$ defined in (8). To obtain the power transfer curve, we will calculate the input power from I_g and the output power from V_{AG2}. Thus, no optimization is required. This is because AG_1 is controlled by AG_2. To calculate the solution curve versus any other parameter μ_1, such as $\mu_1 = \omega$, we will perform a double sweep in μ_1 and V_{AG2} and trace the contour plot of the corresponding I_g value. Note that instead of two nonlinear charges, we may consider two complete nonlinear blocks, as shown in the following example. Then, instead of $j\omega Q_i^1$ we will consider the total block currents I_i^1.

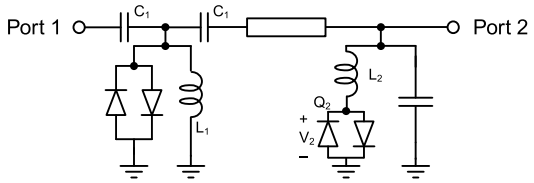

Fig. 2. Lorentzian–Fano nonlinear isolator [1]. Skyworks SMV1232 diodes ($C_{jo} = 4.2$ pF).

III. Lorentzian–Fano Nonlinear Isolator

The works in [1], [2], and [3] have proposed a nonreciprocal isolator based on the coupling through a transmission line of two nonlinear resonators of Lorentzian and Fano types (see Fig. 2). The series branch of this resonator, ideally composed by a nonlinear charge Q_2 and L_2, gives rise to a transmission zero at ω when the following condition is fulfilled:

$$V_T = V_2^1 + jL_2\omega j\omega Q_2^1(\overline{V}_2) = 0. \tag{9}$$

Due to the presence of the Lorentzian resonator, condition (9) will be fulfilled for different input-power values when driving the system through Ports 1 and 2. The operation will also depend on the Lorentzian (parallel) resonance and the additional Fano resonance with C_2. To better evidence the main characteristics of the behavior, we will initially neglect the diode losses, as in [1], [2], and [3].

The circuit in Fig. 2 has been analyzed at 900 MHz by applying the new substitution method in commercial software. When introducing the input signal through Port 1, the independent AG (AG_2) is connected in parallel with the Fano resonator and the current-controlled AG (AG_1) is connected in parallel with the Lorentzian one. Fig. 3(a) presents the results obtained when the electrical length of the transmission line is $\theta = 90°$. They are compared with those provided by default HB, which undergoes discontinuous jumps. In the two cases, we have considered NH = 7 harmonic terms. The jumps obtained in HB (when increasing and decreasing P_{in}) do not allow inferring the actual solution curve, which exhibits a narrow loop in the lower power-transfer region. When introducing the input signal through Port 2, the independent AG (AG_2) is connected in parallel with the Lorentzian resonator and the current-controlled AG (AG_1) is connected in parallel with the Fano one. The results are shown in Fig. 3(b). Default HB gives rise to a discontinuous jump before reaching the turning point, which is due to the ill-conditioning of the HB system. Note that one can predict the low-transfer section using a single AG, in parallel with the nonlinear block of the Fano side. This is because near the Fano series resonance, the voltage amplitude in the Lorentzian resonator will be low. Fig. 3(c) compares the responses obtained when introducing the signal through Ports 1 and 2. In comparison with previous works, the advantage of the new method is the capability to accurately predict the behavior in realistic circuits, such as the one in Fig. 2. The method is also applicable in commercial HB.

As gathered from Fig. 3(c), the P_{in} difference between the upward jumps when injecting through Ports 1 and 2 is insufficient. As shown in [1], [2], and [3], one should be able to improve the response by using a shorter transmission line.

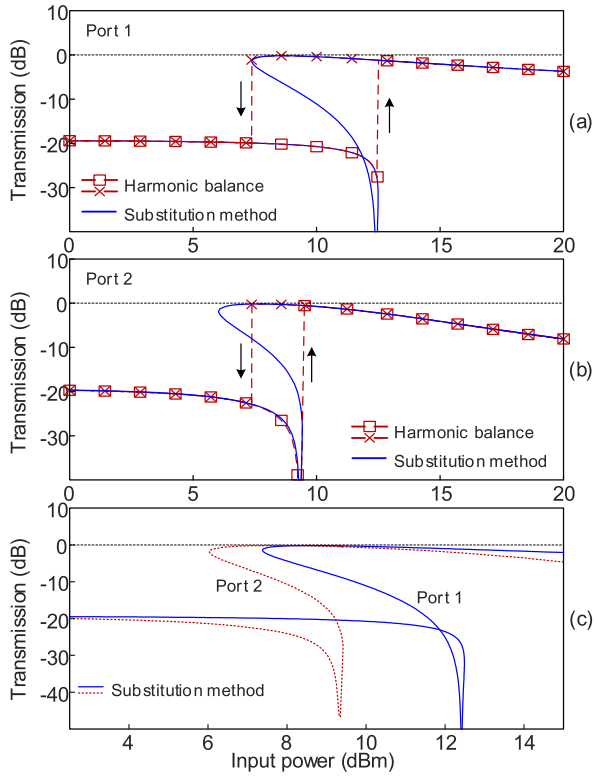

Fig. 3. Electrical length $\theta = 90°$. Comparison of the new method with default HB, considering, in the two cases, NH = 7 harmonic terms. When introducing the signal through (a) Port 1 and (b) Port 2. (c) Predicted nonreciprocal behavior.

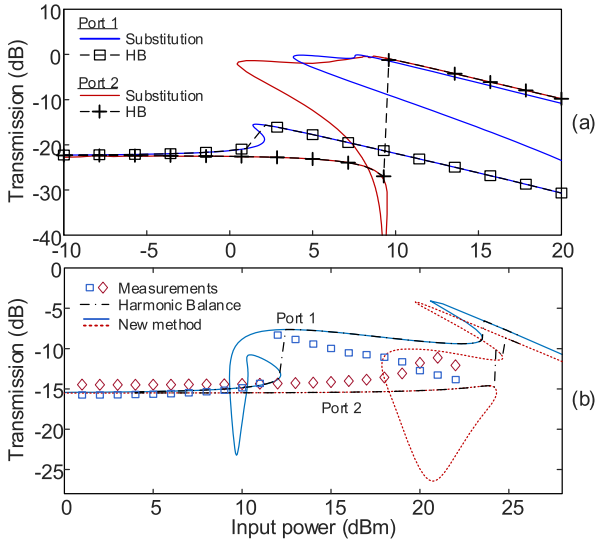

Fig. 4. (a) Comparison of the new method with default HB for $\theta = 10°$, with and without losses. The signal is introduced through Ports 1 and 2. (b) Comparison with measurements and default-HB, when considering detailed models of the diodes and other elements.

Fig. 4(a) compares the results of the new method and default HB for $\theta = 10°$. When introducing the signal through Port 1, there is no jump to the low-loss section. However, when introducing the signal through Port 2, the low-loss section is reached for $P_{\text{in}} = 9.3$ dBm. To compare with measurements, we have considered detailed models of the diodes and other circuit elements, and $\theta = 60°$. The results are shown in Fig. 4(b). The behavior is even more complex; some curve sections are, of course, unstable (unphysical). Note that no optimization of the system performance has been carried out,

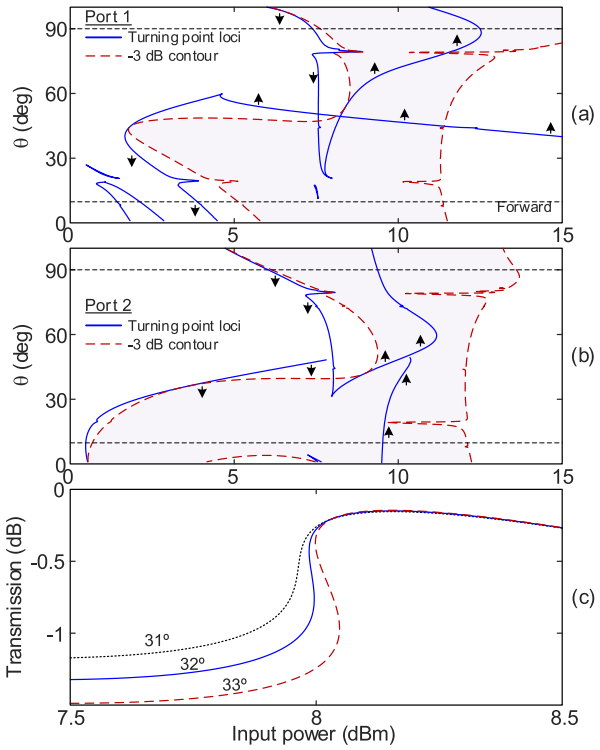

Fig. 5. Turning-point loci (solid blue) in the plane defined by P_{in} and θ. The contour corresponding to a transmission loss of 3 dB is represented in red (dashed). When introducing the signal through (a) Port 1 and (b) Port 2. (c) Validation of the additional hysteresis loop predicted in (b).

since the goal is the accurate prediction of the solution curves. The results of the new method are also compared with the default HB which misses significant parts of the solution curves. We should emphasize that the only reliable validation of the method is the comparison with default HB, since in the two cases we have identical descriptions of all the circuit elements. As stated, the goal is to demonstrate the method capability to address complex multivalued solutions.

IV. Hysteresis Loops

The new formulation based on a single control variable facilitates the calculation of the turning-point locus in the plane defined by any pair of parameters μ_1 and V_{AG2}. The advantage is that, instead of requiring two independent complex variables, the analysis can be carried out with only one. This is shown in two steps. First, we split (7) into real and imaginary parts, and calculate the Jacobian matrix with respect to V_{AG2} and ϕ. Then, we replace the phase-dependent terms with their expressions in terms of $\text{Re}(H)$ and $\text{Im}(H)$. This provides the condition

$$\partial |H(V_{\text{AG2}}, \mu_1)| / \partial V_{\text{AG2}} = 0. \tag{10}$$

To obtain the turning point locus in the plane defined by any two parameters μ_1 and μ_2, at a given I_g, we will perform a triple sweep on μ_2 (external) and μ_1 and V_{AG}. For each μ_2, we will obtain the intersection points of (10) and (8), the latter calculated at the particular I_g. This will help choose μ_2 to get the turning points (boundaries of the hysteresis loops) at suitable values of μ_1.

For a detailed comparison with the solution curves, we will use the idealized models shown in Figs. 3 and 4(a). When introducing the signal through Port 1 and considering the two

parameters P_{in} and θ, one obtains the results in Fig. 5(a), where the turning-point loci are traced in blue. There are several of these loci because for certain θ intervals there is more than one hysteresis loop [see Fig. 4(a)]. The upward and downward jumps in the loci that give rise to significant transmission changes are indicated by arrows. In each case, the right section of the locus corresponds to the upward jump (transition from high loss to low loss). The one on the left corresponds to the downward jump. The horizontal dashed lines correspond to the two θ values in Figs. 3(a) and 4(a). All the turning points are accurately predicted. As has been verified, the small narrow curves also give rise to turning points. We have added the contour corresponding to a transmission loss of 3 dB (in red dashed line). Within this contour, the transmission loss is smaller than 3 dB. For a short θ, the upward jump is not reached, in consistency with Fig. 4(a). Fig. 5(b) presents the loci and 3 dB contour obtained when introducing the signal through Port 2. For low θ there is a single big-transition locus. From $\theta = 31.5°$ up to approximately 45°, another locus gives rise to a small magnitude hysteresis cycle in the upper section of the transfer curve, as validated in Fig. 5(c), which presents a zoom-in view for $\theta = 31°$, 32°, and 33°. The generation of the hysteresis loop from a cusp [14] is accurately predicted. Note that exhaustively obtaining all the turning-point loci through continuation methods (as would be done in a dedicated in-house software) would be virtually impossible due to the need to individually initialize all the disconnected loci.

V. Conclusion

A new analysis method for circuits containing two nonlinear resonators has been presented. The multivalued solution curves are obtained through a substitution method based on the use of AGs that enables the control of the system through a single excitation variable. The method, compatible with the use of commercial HB, requires the introduction of an independent AG and a current-dependent AG. It enables a simple calculation of the turning-point loci in the plane defined by two arbitrary parameters.

References

[1] D. L. Sounas, J. Soric, and A. Alù, "Broadband passive isolators based on coupled nonlinear resonances," *Nature Electron.*, vol. 1, no. 2, pp. 113–119, Feb. 2018.

[2] A. Kord, D. L. Sounas, and A. Alù, "Microwave nonreciprocity," *Proc. IEEE*, vol. 108, no. 10, pp. 1728–1758, Oct. 2020.

[3] M. Cotrufo, S. A. Mann, H. Moussa, and A. Alù, "Nonlinearity-induced nonreciprocity—Part II," *IEEE Trans. Microw. Theory Techn.*, vol. 69, no. 8, pp. 3584–3597, Aug. 2021.

[4] R. Chai and A. Mortazawi, "A position-insensitive wireless power transfer system employing coupled nonlinear resonators," *IEEE Trans. Microw. Theory Techn.*, vol. 69, no. 3, pp. 1752–1759, Mar. 2021.

[5] M. Pandit, C. Zhao, G. Sobreviela, S. Du, X. Zou, and A. Seshia, "Utilizing energy localization in weakly coupled nonlinear resonators for sensing applications," *J. Microelectromech. Syst.*, vol. 28, no. 2, pp. 182–188, Apr. 2019.

[6] V. Rizzoli and A. Neri, "State of the art and present trends in nonlinear microwave CAD techniques," *IEEE Trans. Microw. Theory Techn.*, vol. MTT-36, no. 2, pp. 343–356, Feb. 1988.

[7] R. Quere, E. Ngoya, M. Camiade, A. Suarez, M. Hessane, and J. Obregon, "Large signal design of broadband monolithic microwave frequency dividers and phase-locked oscillators," *IEEE Trans. Microw. Theory Techn.*, vol. 41, no. 11, pp. 1928–1938, Nov. 1993.

[8] R. C. Melville and A. Suárez, "Experimental investigation of bifurcation behavior in nonlinear microwave circuits," *IEEE Trans. Microw. Theory Techn.*, vol. 65, no. 5, pp. 1545–1559, May 2017.

[9] A. Suarez, *Analysis and Design of Autonomous Microwave Circuits*. Hoboken, NJ, USA: Wiley, 2009.

[10] F. Ramirez, J. L. Garcia H, T. Fernandez, and A. Suarez, "Nonlinear simulation techniques for the optimized design of push–push oscillators," in *IEEE MTT-S Int. Microw. Symp. Dig.*, Philadelphia, PA, USA, Jun. 2003, pp. 2157–2160.

[11] A. Suarez, A. Collado, and F. Ramirez, "Harmonic-balance techniques for the design of coupled-oscillator systems in both unforced and injection-locked operation," in *IEEE MTT-S Int. Microw. Symp. Dig.*, Long Beach, CA, USA, Jun. 2005, pp. 887–890.

[12] V. Ardila, F. Ramirez, and A. Suarez, "Analytical and numerical bifurcation analysis of circuits based on nonlinear resonators," *IEEE Trans. Microw. Theory Techn.*, vol. 69, no. 10, pp. 4392–4405, Oct. 2021.

[13] S. Hernandez and A. Suarez, "Systematic methodology for the global stability analysis of nonlinear circuits," *IEEE Trans. Microw. Theory Techn.*, vol. 67, no. 1, pp. 3–15, Jan. 2019.

[14] J. Guckenheimer and P. J. Holmes, *Nonlinear Oscillations, Dynamical Systems, and Bifurcations of Vector Fields*. New York, NY, USA: Springer, 1983.